Direct deposition strategy for highly ordered inorganic organic perovskite thin films and their optoelectronic applications

Shahab Ahmad, Chintam Hanmandlu, Pawan K. Kanaujia and G. Vijaya Prakash*

Nanophotonics lab, Department of Physics, Indian Institute of Technology Delhi, New Delhi-110016, India
*prakash@physics.iitd.ac.in

Abstract: A direct deposition methodology has been optimized for highly crystalline inorganic-organic (IO) perovskite thin films. The simplest deposition ensures long-range order with high *c*-oriented thin films, thicknesses ranging from ultra-thin (~20nm) and upto 1.5 μm. These self-assembled layered perovskites are naturally aligned alternative stacking arrangement of inorganic and organic monolayers, resemble multiple quantum wells (MQWs), which offers superior optoelectronic properties such as room-temperature optical excitons, strong electrically induced photo-carrier mobilities etc. The established fabrication is having device-compatible advantage over other conventional solution–processed thin films wherein the optical features are restricted by thickness limitations (<200nm) and with possible corrugated surface morphologies with multi-phases. The universally acceptable ability has been demonstrated for wide varieties of organic moieties (R) as well as different lead halide networks in type (R-NH_3)$_2$$PbX_4$ (X = I, Br,Cl).The potential of the direct deposition is demonstrated for 3D template structure fabrication as well as in photocurrent response capability.

©2014 Optical Society of America

References and links

1. N. G. Park, "Organometal perovskite light absorbers toward a 20% efficiency low-cost solid-state mesoscopic solar cell," J. Phys. Chem. Lett. **4**(15), 2423–2429 (2013).
2. H. J. Snaith, "Perovskites: the emergence of a new era for low-cost, high- efficiency solar cells," J. Phys. Chem. Lett. **4**(21), 3623–3630 (2013).
3. M. Era, S. Morimoto, T. Tsutsui, and S. Saito, "Organic-inorganic heterostructure electroluminescent device using a layered perovskite semiconductor ($C_6H_5C_2H_4NH_3$)$_2$$PbI_4$," Appl. Phys. Lett. **65**(6), 676–678 (1994).
4. K. Pradeesh, J. J. Baumberg, and G. V. Prakash, "Strong exciton-photon coupling in inorganic-organic multiple quantum wells embedded low-Q microcavity," Opt. Express **17**(24), 22171–22178 (2009).
5. D. B. Mitzi, "Templating and structural engineering in organic–inorganic perovskites," J. Chem. Soc. Dalton **1**(1), 1–12 (2001).
6. D. B. Mitzi, K. Chondroudis, and C. R. Kagan, "Organic–inorganic electronics," IBM J. Res. Develop. **45**(1), 29–45 (2001).
7. D. B. Mitzi, C. A. Feild, W. T. A. Harrison, and A. M. Guloy, "Conducting tin halides with a layered organic-based perovskite structure," Nature **369**(6480), 467–469 (1994).
8. N. Kitazawa, "Optical absorption and photoluminescence properties of Pb(I, Br)-based two-dimensional layered perovskite," Jpn. J. Appl. Phys. **36**(Part 1, No. 4A), 2272–2276 (1997).
9. Z. Xu and D. B. Mitzi, "[CH_3(CH_2)$_{11}$$NH_3$]$SnI_3$: a hybrid semiconductor with MoO_3-type tin(II) iodide layers," Inorg. Chem. **42**(21), 6589–6591 (2003).
10. C. R. Kagan, D. B. Mitzi, and C. D. Dimitrakopoulos, "Organic-inorganic hybrid materials as semiconducting channels in thin-film field-effect transistors," Science **286**(5441), 945–947 (1999).
11. D. B. Mitzi, S. Wang, C. A. Feild, C. A. Chess, and A. M. Guloy, "Conducting layered organic-inorganic halides containing (110)-oriented perovskite sheets," Science **267**(5203), 1473–1476 (1995).
12. E. A. Muljarov, S. G. Tikhodeev, N. A. Gippius, and T. Ishihara, "Excitons in self-organized semiconductor/insulator superlattices: PbI-based perovskite compounds," Phys. Rev. B Condens. Matter **51**(20), 14370–14378 (1995).

13. M. Shimizu, J. Fujisawa, and J. Ishi-Hayase, "Influence of dielectric confinement on excitonic nonlinearity in inorganic-organic layered semiconductors," Phys. Rev. B **71**(20), 205306 (2005).
14. C. C. Stoumpos, C. D. Malliakas, and M. G. Kanatzidis, "Semiconducting tin and lead iodide perovskites with organic cations: phase transitions, high mobilities, and near-infrared photoluminescent properties," Inorg. Chem. **52**(15), 9019–9038 (2013).
15. M. M. Lee, J. Teuscher, T. Miyasaka, T. N. Murakami, and H. J. Snaith, "Efficient hybrid solar cells based on meso-superstructured organometal halide perovskites," Science **338**(6107), 643–647 (2012).
16. J. H. Heo, S. H. Im, J. H. Noh, T. N. Mandal, C. Lim, J. A. Chang, Y. H. Lee, H. Kim, A. Sarkar, M. K. Nazeeruddin, M. Gra¨tzel, and S. I. Seok, "Efficient inorganic-organic hybrid heterojunction solar cells containing perovskite compound and polymeric hole conductors," Nat. Photonics **7**(6), 486–491 (2013).
17. S. D. Stranks, G. E. Eperon, G. Grancini, C. Menelaou, M. J. P. Alcocer, T. Leijtens, L. M. Herz, A. Petrozza, and H. J. Snaith, "Electron-hole diffusion lengths exceeding 1 micrometer in an organometal trihalide perovskite absorber," Science **342**(6156), 341–344 (2013).
18. Q. Chen, H. Zhou, Z. Hong, S. Luo, H. S. Duan, H. H. Wang, Y. Liu, G. Li, and Y. Yang, "Planar heterojunction perovskite solar cells via vapor-assisted solution process," J. Am. Chem. Soc. **136**(2), 622–625 (2014).
19. T. Matsui, A. Yamaguchi, Y. Takeoka, M. Rikukawa, and K. Sanui, "Fabrication of two-dimensional layered perovskite [NH$_3$(CH$_2$)$_{12}$NH$_3$]PbX$_4$ thin films using a self-assembly method," Chem. Commun. (Camb.) **10**(10), 1094–1095 (2002).
20. D. B. Mitzi, D. R. Medeiros, and P. W. DeHaven, "Low-temperature melt processing of organic-inorganic hybrid films," Chem. Mater. **14**(7), 2839–2841 (2002).
21. K. Ikegami, "Spectroscopic study of J aggregates of amphiphilic merocyanine dyes formed in their pure Langmuir films," J. Chem. Phys. **121**(5), 2337–2347 (2004).
22. K. Pradeesh, J. J. Baumberg, and G. Vijaya Prakash, "In situ intercalation strategies for device-quality hybrid inorganic-organic self-assembled quantum wells," Appl. Phys. Lett. **95**(3), 033309 (2009).
23. Y. Sawada and M. Suzuki, "Thermal change of SnI$_2$ thin films. Part 4: TG-DTA and DSC," Thermochim. Acta **254**, 261–266 (1995).
24. M. Era, T. Hattori, T. Taira, and T. Tsutsui, "Self-organized growth of PbI-based layered perovskite quantum well by dual-source vapor deposition," Chem. Mater. **9**(1), 8–10 (1997).
25. D. B. Mitzi, M. T. Prikas, and K. Chondroudis, "Thin film deposition of organic-inorganic hybrid materials using a single source thermal ablation technique," Chem. Mater. **11**(3), 542–544 (1999).
26. T. Ishihara, J. Takahashi, and T. Goto, "Optical properties due to electronics transitions in two-dimensional semiconductors (C$_n$H$_{2n+1}$NH$_3$)$_2$PbI$_4$," Phys. Rev. B **42**(17), 11099–11107 (1990).
27. I. B. Koutselas, L. Ducasse, and G. C. Papavassiliou, "Electronic properties of three-and low-dimensional semiconducting materials with Pb halide and Sn halide units," J. Phys. Condens. Matter **8**(9), 1217–1227 (1996).
28. M. Hirasawa, T. Ishihara, and T. Goto, "Exciton features in 0-, 2-, and 3-dimensional networks of [PbI$_6$]$^{4-}$ octahedra," J. Phys. Soc. Jpn. **63**(10), 3870–3879 (1994).
29. J. Burschka, N. Pellet, S. J. Moon, R. Humphry-Baker, P. Gao, M. K. Nazeeruddin, and M. Grätzel, "Sequential deposition as a route to high-performance perovskite-sensitized solar cells," Nature **499**(7458), 316–319 (2013).
30. K. Pradeesh, J. J. Baumberg, and G. Vijaya Prakash, "Exciton switching and Peierls transitions in hybrid inorganic-organic self-assembled quantum wells," Appl. Phys. Lett. **95**(17), 173305 (2009).
31. K. Pradeesh, K. Nageswara Rao, and G. Vijaya Prakash, "Synthesis, Structural, Thermal and Optical Studies of Inorganic-Organic Hybrid Semiconductors, R-PbI$_4$," J. Appl. Phys. **113**(8), 083523 (2013).
32. S. Ahmad and G. Vijaya Prakash, "Two-step fabrication of R-PbI$_{4(1-y)}$Br$_{4y}$ type light emitting inorganic-organic hybrid photonic structures," Opt. Mater. Express **4**(1), 101–110 (2014).
33. S. Ahmad and G. V. Prakash, "Strong room-temperature UV to red excitons from inorganic organic layered perovskites, (R-NH$_3$)$_2$MX$_4$ (M=Pb^{2+}, Sn^{2+}, Hg^{2+}; X=I$^-$, Br$^-$)," J. Nanophotonics **8**(1), 083892 (2014).
34. Z. Y. Cheng, Z. Wang, R. B. Xing, Y. C. Han, and J. Lin, "Patterning and photoluminescent properties of perovskite-type organic/inorganic hybrid luminescent films by soft lithography," Chem. Phys. Lett. **376**(3-4), 481–486 (2003).
35. Y. Jun, P. Nagpal, and D. J. Norris, "Thermally stable organic–inorganic hybrid photoresists for fabrication of photonic band gap structures with direct laser writing," Adv. Mater. **20**(3), 606–610 (2008).
36. G. Grosso, J. Graves, A. T. Hammack, A. A. High, L. V. Butov, M. Hanson, and A. C. Gossard, "Excitonic switches operating at around 100 K," Nat. Photonics **3**(10), 577–580 (2009).
37. G. Xing, N. Mathews, S. Sun, S. S. Lim, Y. M. Lam, M. Grätzel, S. Mhaisalkar, and T. C. Sum, "Long-range balanced electron- and hole-transport lengths in organic-inorganic CH$_3$NH$_3$PbI$_3$," Science **342**(6156), 344–347 (2013).
38. S. Ahmad, J. J. Baumberg, and G. Vijaya Prakash, "Structural tunability and switchable exciton emission in inorganic-organic hybrids with mixed halides," J. Appl. Phys. **114**(23), 233511 (2013).

1. Introduction

Naturally self-assembled inorganic-organic (IO) perovskites are attractive highly crystalline hybrids, providing a new opportunity to structurally engineer inorganic semiconductor and organic entities into a single material. These hybrid perovskites takes the advantage that combine distinct properties of inorganic and organic components within a single molecular material. These IO perovskites are thermally, mechanically and thermodynamically stable and

are most competitive candidates for various photonic and optoelectronic device applications [1–4]. Depending on the nature of organic moiety, the 3D networks of AMX_3 type IO perovskite structures (A = amino-end group organic moiety, M = Pb^{2+}, Sn^{2+} and X = I^-, Br^- and Cl^-) can be controllably fabricated into 0-, 1-, 2-, or 3-dimensional entities [5–11]. Among them, the two-dimensional (2D) layered perovskites of $(R-NH_3)_2MX_4$ type, adopts alternate *c*-axis stacks of semiconducting MX_6 octahedra sheets *(wells)* and bi-layers of organic entities *(barriers)* and are considered to be naturally self-assembled multiple quantum wells (MQWs) [Fig. 1(a)]. The low dimensionality and large dielectric mismatch ($\varepsilon_{org}<\varepsilon_{inorg}$) in 2D pervoksites, results into large exciton binding energies enabling strong *Mott* type excitons observable even at room-temperature [12,13]. These systems have recently emerged as highly-promising new systems for applications such IO-LEDs, thin-film transistors (IO-TFTs), solar cells, nonlinear switches, etc. The low-temperature (77K) operated LED from layered PbI_4^{2-} based IO perovskite LEDs showed electroluminescence [3] intensities up to 10,000 cd/m^2 and SnI_4^{2-} based IO-TFTs showed highest field-effect mobilities [10] up to 0.60 cm^2/V-s along with current modulation more than 10^4. Similarly the usage of three-dimensional (3D) cage type IO perovskite, $CH_3NH_3PbI_3$ has recently demonstrated tremendous improvement in the performance of heterojunction solar cells with power conversion efficiencies up to 15% [14–18]. The IO perovskites, in general, are synthesized from conventional chemical reactions and corresponding devices are fabricated using solution based methods such as spin-coating, intercalation method, Langmuir Blodgett, layer-by-layer self-assembly [15–22]. However, for large-scale optoelectronic integration into devices, solution-based fabrication methodologies may not be compatible and the processing is always tricky and require special fabrication conditions (such as glove box, inert atmosphere etc.), depending on the nature of organic moieties and inorganic constituents (such as air sensitive SnI_2) [9,23]. Also, the bottleneck to obtain strong room-temperature excitons is the constraint of thickness limits (typically 100-150nm) in all the aforementioned deposition methods. Vacuum compatible deposition has been demonstrated by evaporating the inorganic and organic moieties in two separate boats [24]. While the method successfully demonstrated the IO perovskite deposition, the resulted films are defective and disordered in nature, due to difficulty in balancing the simultaneous evaporation rates. Similarly Mitzi *et al*. reported a single source thermal ablation for some set of IO perovskites [25], using IO perovskite suspensions/solution dried tantalum boats. The resultant film thicknesses (typically <200nm) are controlled by initial volumes and the surface roughness is comparable to the spin-coated films.

While solid-state deposition is highly desirable, one of the experimental difficulties with IO perovskite is that the organic moiety may decompose and/or dissociate at very lower temperatures compared to that of inorganic counterpart. Moreover, to implement a direct deposition method for device fabrication, a systematic optimization of deposition conditions to achieve long-range order with thickness control and applicability for wide range of IO perovskite family is highly essential. Here, a straight forward methodology of direct deposition of high-quality thin films has been successfully demonstrated and the fabrication conditions are optimized for wide varieties of layered (2D) IO perovskites from the family of $(R-NH_3)_2PbI_4$. The precise control over thickness with relative smoothness along with long-range order has been optimized. The potential application in prototype photonic/optoelectronics device fabrication and carving them into macroscopic shapes has also been exemplified.

2. Experiment

Synthesis of several varieties of polycrystalline IO perovskite powders of $(R-NH_3)_2PbX_4$ [X = I, Br, Cl] type were carried out by solution chemistry based conventional sol-gel method. Firstly, lead halide (PbX_2) has been dissolved in concentrated aqueous HX (X = I, Br, Cl) in the stoichiometric quantities and kept on heating at 60°C under constant stirring. Once the lead halide is completely dissolved in HX, organic moiety ($R-NH_2$) has been added drop-wise to the solution in stoichiometric ratio. The resultant solution was allowed to rest at 60°C for an

hour and then cooled slowly to room-temperature without stirring. The reaction ends with the formation of IO perovskite in the form of precipitates which were extracted and kept for drying for further purification. The pellets of dry IO perovskite powders have been prepared under low pressure without using any organic binder. These pellets are directly used for film deposition at vacuum of ~5 x 10^{-5} torr on to glass substrate by passing swift currents of 100 to 190A (using molybdenum boat) within short duration (<10 sec). The synthesized products and deposited films were carefully stored in inert atmosphere until further use. All the characterizations are carried out in standard ambient conditions.

Thin film absorption measurements were carried out using a white light source (DH-2000, Mikropack) coupled to a high resolution fiber optic spectrometer (USB 2000, Ocean Optics). Photoluminescence (PL) measurements were carried out using specific excitation source (410nm diode laser, 337nm N_2 laser and 288nm Xe-lamp source) and the emission is coupled into a monochromator coupled with a PMT (Acton, Princeton Instruments) or fiber-optic spectrometers, using appropriate filters. The PL images and spectral line scans are obtained from modified microscope (BX-51, Olympus) equipped with XY-piezo stage (Marzhauser Wetzlar), 410nm diode laser (<50mW) and fiber-optic spectrometer using a long-pass (λ>425nm) filter. Glancing angle thin film X-Ray Diffraction studies were carried out in the 2θ range from 3° to 40° with Cu Kα radiation (λ = 1.5406 Å) using X'Pert Pro, Panalytical. The thickness was continuously monitored during deposition and the same has been confirmed by a thickness profiler. Atomic force microscopy measurements were performed using Dimension Icon ScanAsyst, Bruker. Photocurrent measurements are performed using Xe lamp source coupled to a monochromator (TMc 300, Bentham) and digital nano-ammeter and D.C. voltage source.

3. Results and discussion

3.1 IO perovskite direct deposition parameter optimization

Large thermal currents and rapid evaporation does not allow organic moiety decomposition/dissociation and at the same time provides required temperature for evaporation of inorganic species. Hence, both organic and inorganic evaporates together with similar rates and eventually self-assemble onto the substrate, placed at fixed height (~15cm) above the molybdenum boat. The optimization of the film deposition has been demonstrated for one of the IO perovskite, CHPI (Cyclohexenyl ethyl ammonium lead iodide, $(C_6H_9C_2H_4NH_3)_2PbI_4$) [Fig. 1(a)]. Wide range of film thickness has been achieved by controlling the evaporating material volume and varying the current between 100 and 190A for a constant exposure time of 10 sec. It must be noted that no film growth has been observed for less than the minimum current range mentioned above. Thus such wide range of currents provides sufficient heating rates for rapid evaporation. The presence of strong *(00l)* characteristic reflections in the thin film XRD patterns signifies the presence of strong alternate stacking of inorganic (infinitely extended PbI_6 corner-shared octahedral) sheets and organic ($(R-NH_3)^-$) bilayers [6] with uniform growth in a single phase, even to high thicknesses upto ~1500nm [Fig. 1(b)].
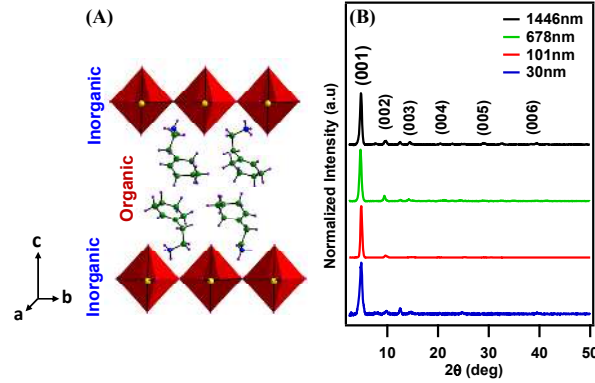
Fig. 1. (a) Shows the schematic crystal structure packing representation of typical ($C_6H_9C_2H_4NH_3)_2PbI_4$ [CHPI] layered perovskite, viewed along *b*-direction. (b) XRD patterns of as direct deposited CHPI films of various thicknesses.

As a consequence of natural MQWs features, all directly deposited IO perovskite films show strong room-temperature exciton photoluminescence (PL) (λ_{ex}~410nm, FWHM ~20nm) [Fig. 2(a)]. In these systems, amino based organic moiety (R-NH$_3$)$^-$, the exfoliating agent, is a non-emitting material with relatively large bandgap (>4.5eV), therefore the room-temperature optical exciton features are *Mott* type confined within inorganic counterpart [8]. The strong emission within the PbI$_4^{2-}$ inorganic network has been attributed to exciton transitions between the lowest conduction band, composed mainly of Pb(*6p*) atomic orbitals and the top of the valence band, contains an admixture of Pb(*6s*) and I(*5p*) orbital [26–28]. As a point of note, the films fabricated from other conventional solution processing, such as intercalation method [22] shows unusual exciton peak shifts (shown by cross symbols in Fig. 2(b)), non-reproducibility, spectral broadening and red-end broad defect induced emissions [4,6,22] Whereas in these directly deposited films, the exciton PL peak positions and intensities are almost invariant from 350nm thick film even upto micron thicknesses [Fig. 2(b) and 2(c)]. Moreover the conventional films, formed by relatively slower self-assembly process, show limited range of thicknesses with a critical upper limit of ~150nm and beyond this limit, the film result into poly crystalline films of corrugated surfaces with pronounced defect/crystal edge emissions [16,18,29] The possible peak shift and defect related emission are due to crumpling of inorganic layers resulted either by heaviness or random/disordered conformation of organic moieties [4,22]. In the present case the fabricated films, even up to micron thickness, have shown uniform surface quality with uniformly consistent exciton PL features suggesting that self-assembly of MQWs during direct deposition is more advantageous for device applications than other solution processing methods.
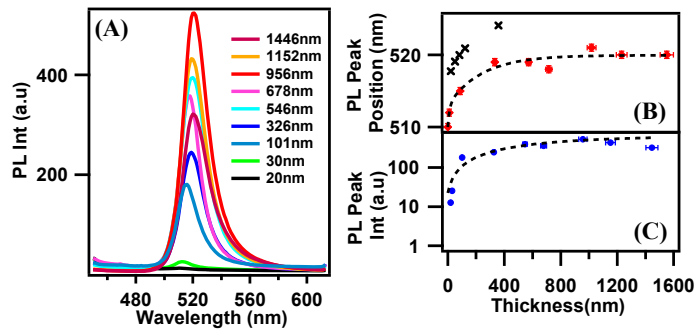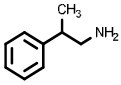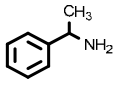
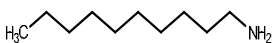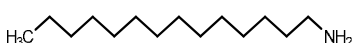

Fig. 2. (a) PL spectra (λex~410nm) of direct deposited CHPI films of various thicknesses. (b) and (c) shows the corresponding PL peak position and PL peak intensity variation with thickness respectively. (The data represented in cross symbol in (b) is obtained for solution processed (intercalation) films, having thickness limitations [22]).

The universal acceptability of direct deposition has been demonstrated for wide range of IO perovskites containing (a) different varieties of organic moieties ranging from cyclic (aryl) to long alkyl ammonium carbon chain based organics (Table 1) and (b) different metal halide networks such as $PbBr_4^{2-}$ and $PbCl_4^{2-}$. Figure 3(a) exemplifies the XRD patterns of some of the fabricated $(R-NH_3)_2PbI_4$ type IO perovskite thin films (~100nm) containing several varieties of organic moieties. Here MPPI, PEPI and CHPI contains cyclic (aryl) type organics with R = $C_6H_5CH(CH_3)CH_2$-, $C_6H_5C_2H_4$- and $C_6H_9C_2H_4$- respectively and C7PI, C9PI, C10PI, C12PI and C14PI are based on long alkyl ammonium carbon chain with a general formula of $(C_nH_{2n+1}NH_2)^-$ where n = 7, 9, 10, 12 and 14 respectively. Deposition of another 2D IO perovskite, OLPI $[((CH_2)_7CH = CH(CH_2)_8NH_3)_2PbI_4]$, based on long alkyl chain based organic moiety oleylamine has also been demonstrated.

Table 1. The empirical names and chemical formulae of various cyclic and long carbon chain group based organic moieties and corresponding synthesized IO-perovskite.

Organic	Organic Structure	IO perovskite
β-Methylphenethylamine		MPPI [(C_6H_5CH(CH_3)CH_2-NH_3)_2PbI_4]
β-Phenylethylamine		PEPI [(C_6H_5C_2H_4NH_3)_2Pb_4]
2-Cyclohexyl-ethylamine		[(C_6H_9C_2H_4NH_3)_2PbX_4] (X=I, CHPI; X=Br, CHPB, X=Cl, CHPC)
Heptylamine		C7PI [(C_7H_15NH_3)_2PbI_4]
Nonylamine		C9PI [(C_9H_19NH_3)_2PbI_4]
Decylamine		C10PI [(C_10H_21NH_3)_2PbI_4]
Dodecylamine		C12PI [(C_12H_25NH_3)_2PbI_4]
Tetradecylamine		C14PI [(C_14H_29NH_3)_2PbI_4]
Oleylamine		OLPI [((CH_2)_7CH=CH(CH_2)_8NH_3)_2PbI_4]

For all deposited films the presence of strong *(00l)* characteristic peaks in XRD patterns suggests the well-stacked IO perovskites along *c*-axis, without any defects or impurities. Here, the XRD pattern of thermal vapour deposited PbI_2 thin film is shown for phase comparison. The absence of PbI_2 characteristic peak *(001)* in all perovskite film XRD patterns again confirms the well self-assembled inorganic and organic alternate layering arrangement. As observed in the characteristic peak *(002)* of XRD patterns of long alkyl ammonium carbon chain based IO hybrids, the interlayer *d*-spacing is decreasing monotonically from d_{002}~29.195 Å to 19.888 Å with decrease in the size of the carbon chain length of organic moiety from n = 14 to 7 respectively.

Apart from quantum and dielectric confinement effects, the optical exciton energies are strongly dependent on several intriguing structural features. The variation of organic moieties cause disorder due to conformation into parent inorganic matrix (for example, long alkyl chain conformation into PbI_4 network as disordered Gauche isomers).i.e., Pb-I-Pb in-plane bonding angles in the extended network of PbI_6 octahedron [5,30,38]. Due to different

conformation/tagging of organics with two infinitely extended Pb-I network layers, the Pb-I-Pb inorganic network bond lengths/angles and inter-connectivity within the infinitely extended PbI_6 octahedral units (corner/edge sharing) are widely different. Such structural reorganization within the inorganic network is expected to change the electronic bandgap and consequently the associated excitons as well [31,33]. Figure 3(b) exemplifies the PL spectra obtained from several $(R-NH_3)_2PbI_4$ systems, wherein R is aryl (cyclic) or long alkyl ammonium carbon chain type organic moiety. The PL peak position show distinct tunability of about ~30nm (490nm to 520nm) for various 2D IO hybrids. The detailed discussion about the structural variation (such as in-plane Pb-I-Pb bond angle deformations) due to organic conformation and its direct correlation to the optical bandgap and corresponding exciton PL energies are reported elsewhere [30,31]. It is to mention that the long-alkyl carbon chain based IO perovskites are known for temperature, thickness and ageing dependent structural phase flips (Phase I and Phase II) which causes exciton switching [30]. Here, all directly deposited thin film of $((C_nH_{2n+1}NH_3)_2PbI_4)$ perovskites are predominantly belong to phase II crystal packing (monoclinic).
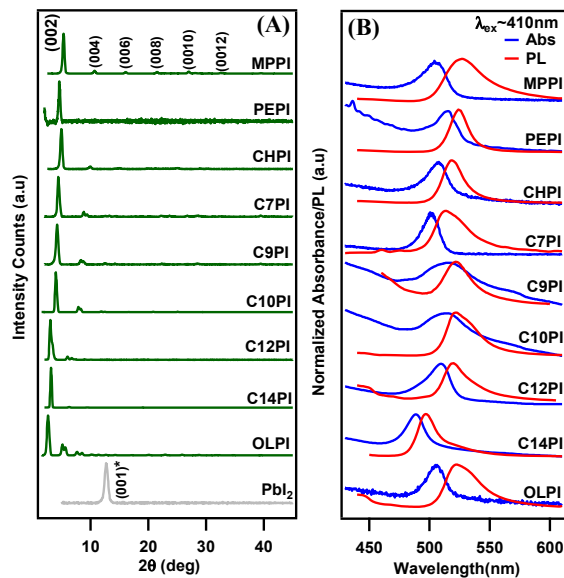

Fig. 3. (a) XRD patterns and corresponding (b) room-temperature exciton absorption and PL spectra of various organic moieties (R = cyclic and long carbon chain) based IO perovskite [(R-NH_3)_2PbI_4] thin films (~100nm). The XRD pattern of PbI_2 is also shown for comparison.

The proposed method further addresses the problem of depositing other metal halide based IO perovskites. Here as an example, thin films from the IO perovskite family of $(C_6H_9C_2H_4NH_3)_2PbX_4$ (X = I (CHPI), Br (CHPB) and Cl (CHPC)) are deposited and their structural and optical features are discussed. It is to note that lead bromide/ chloride based IO perovskites are soluble in non-volatile solvents (such as DMF and DMSO), therefore use of conventional spin coating is a bottleneck for large area thin film fabrication [33]. Regardless of metal halide all the direct deposited films show strong *(00l)* characteristics peaks in XRD patterns demonstrating the *c*-axis oriented growth perpendicular to the substrate [Fig. 4(a)]. The strong exciton features observed for CHPI, CHPB and CHPC at λ_{em}~519nm, 408nm and 360nm indicating that the methodology can be easily adoptable for various IO perovskites for wide range of structural and excitonic tunability [32,33,38].
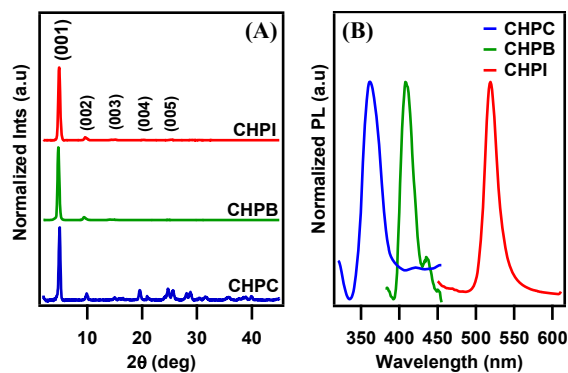
Fig. 4. (a) XRD patterns and corresponding (b) room-temperature exciton PL spectra of direct deposited CHPB and CHPC films (excitation wavelengths are 337nm and 288nm respectively). CHPI is shown for comparison.

3.2 Fabrication of 3D photonic structures

Exponentially growing interests in photonics and optoelectronics has been driven in recent years mostly by novel properties as well as process of device and structure fabrication. The optimized solvent-free direct deposition can be directly adopted for large-scale photonic and optoelectronic device fabrications, such as LEDs, photodetectors and TFTs [3,4,9] The method can also be utilized to create desired 2D/3D wavelength-ordered periodic structures in connection with other methods such as template-assisted growth, lithographic techniques and ion/laser beam writings [34,35]. Here, we demonstrate a simplest template based direct deposition of macro-scaled structures, which can be conveniently extended down to sub-micron structures. The confocal white light (bright field) and PL images [Fig. 5(a) and 5(b)] suggests that the fabricated structures (circular, d = 580μm, thickness ~500nm) are uniform in shape with slight template-screening effect at the edges. However by using appropriate mask design, such screening issues can be avoided. Atomic force microscopy measurement over a central portion area of 25μm^2 also ensures desired surface morphology of roughness below 8nm [Fig. 5(e)].

As addressed previously, the naturally self-assembled IO perovskites are, in general, prone to show strong dependence of optical exciton energies on the structural deformation, crystal defects and thickness [4,22,30]. In this view, the PL spectral line scans are performed along the diameter of these circular 3D-structures of thickness ~500nm, by focusing the excitation laser (410nm, <10mW) and the PL spectra has been collected at the reflected image plane and mapped with 10μm resolution [Fig. 5(a)]. The deposited structures show almost negligible exciton PL peak variation (± 0.2nm) over a large area within central portion of structure [Fig. 5(d)], even for such a highly thick (500nm) structures. For comparison, the exciton PL peak positions in similar template structures of about 100nm thickness fabricated by solution-processing [32], are severely red-shifted at the edges. Therefore, the directly deposited perovskite systems can be easily visualized into wavelength-order photonic structures to exploit the exciton related effects such as exciton optoelectronic transistors and electro-optic switching modulators [36]. While such devices are already known in conventional inorganic MQWs, though mainly for low-temperature performance, utilizing the ability to integrate these natural IO MQWs using established direct deposition would open-up new opportunities for room-temperature properties.
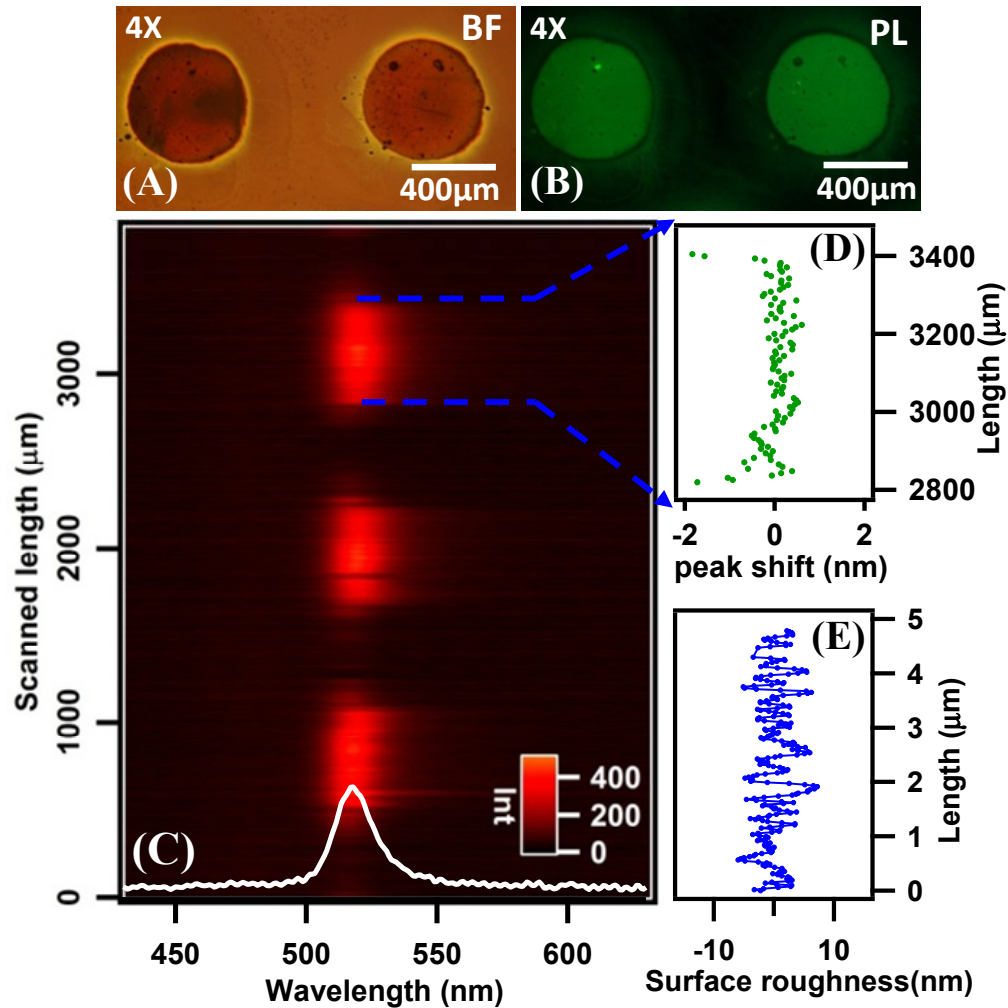
Fig. 5. Confocal microscopic (A) white light (bright field) and (B) PL (λ_{ex}~410 nm, ALP filter>425nm) images of circular 3D structures of $(C_6H_9C_2H_4NH_3)_2PbI_4$ (CHPI) IO perovskite. (C) Room-temperature exciton PL line scan spectral mapping along the diameter of the circular structures, using 410 nm laser excitation (inset shows the PL spectra obtained from the central portion of the structure). (D) PL peak position (λ_{em}~520nm) variation observed along one of the structure. (E) AFM surface roughness line scan over a length of 5μm.

3.3 Direct integration of IO perovskites into prototype photodetector configuration

Another potential passive device property is the exciton carrier transport and the photocurrent response for photovoltaic applications [15–18,29]. Figure 6(a) shows the configuration of a photodetector, realized by depositing the 200nm thick IO perovskite film on patterned transparent conducting substrate (ITO) and depositing Al-metal contacts on the top of IO perovskite film.
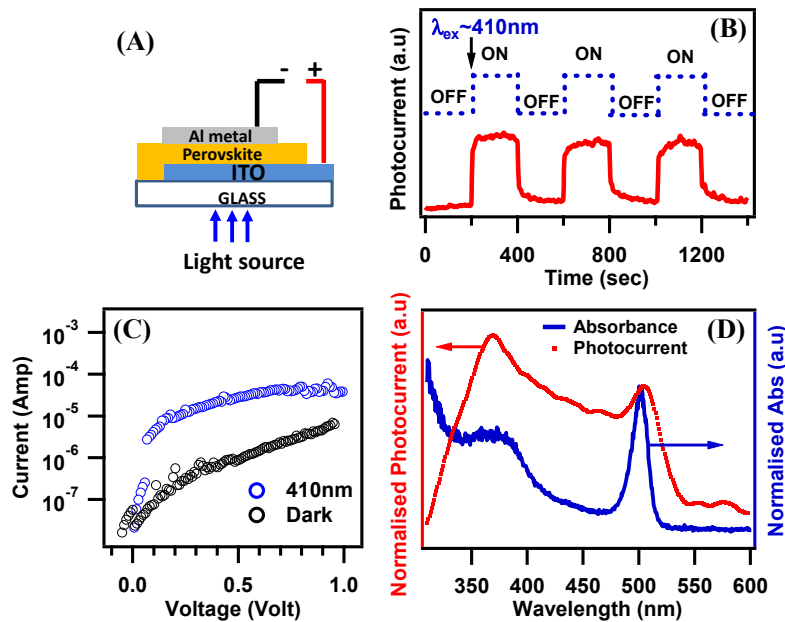
Fig. 6. (a) Schematic representation of photodetector configuration with $(C_7H_{15}NH_3)_2PbI_4$ [C7PI] IO perovskite direct deposited film as active material layer. Room-temperature (b) ON-OFF photocurrent response characteristics recorded under 410nm illumination at 0V bias, (c) current-voltage characteristics under 410nm illumination and dark conditions and (d) photocurrent spectral response plot at 0V bias condition (optical absorption spectra of C7PI is also included for comparison).

The room-temperature photocurrent ON-OFF response has been recorded by illuminating perovskite film using 410nm wavelength from Xe-lamp source (<8mW) [Fig. 6(b)]. The illumination wavelength is above the lowest optical band gap composed of inorganic component (PbI_4^{2-}). The sharp photocurrent response upon the band-to-band excitation shows that the photo induced electron-hole pairs are efficiently generated and collected. It was recently reported [37], that the solution processed IO perovskite possesses long-range electron-hole diffusion lengths of at least 100 nm. Therefore such sharp photocurrent response can be attributed to large diffusion lengths, and further experiments are needed to optimize parameters such as charge-carrier diffusion lengths and charge-carrier life times, in order to utilize these IO perovskites into photovoltaic devices with enhanced power conversion efficiencies. The current-voltage characteristics show typical diode-like behavior with significant enhancement in the photo-carrier collections at higher bias voltages [Fig. 6(c)]. The broad spectral photocurrent (300-550nm) response closely follows the absorption spectral features [Fig. 6(d)]. As in the case of absorption, the photocurrent response also show two distinct regions of interest; a broad band-to-band transition at about 370nm and a sharp exciton feature at about 504nm. However to realize more realistic photovoltaic and photodetector applications from these directly deposited perovskites, further experiments (such as internal photocurrent and quantum efficiencies, robustness of device, careful selection/optimization of metal contacts etc.) are required to compare and correlate relative quantum efficiencies to that of existing solution-processed devices. It is worth pursuing for the large-scale device applications by directly utilizing the solid-state deposition techniques combined with other methods such as UV lithography and direct laser writing. Another advantage is the deposition onto uneven and 3D templated structures and easy integration with other material depositions (such as metal contacts and insulators) [32,36,37].

4. Conclusions

In conclusion, a simple methodology of direct deposition of highly ordered inorganic-organic layered perovskites has been optimized for several varieties of $(R\text{-}NH_3)_2PbX_4$ type systems. Carefully optimized deposition ensures the deposition of several possible structurally different varieties with long-range ordered high thick films (upto 1.5 µm) and also easily achievable 2D/3D wavelength-ordered photonic structure fabrication capabilities. Such smoothness and long-range ordering even at high thicknesses is not easily achievable from other conventional solution processing methods. These IO perovskites possesses strong room-temperature exciton features with potential optoelectronic properties, therefore the demonstrated and optimized methodology can be directly applied for new photonic applications such as IO-LEDs, excitonic switching devices and third-generation photovoltaics.